

# A Generalized Learning Framework for Self-Supervised Contrastive Learning

Lingyu Si<sup>1,2</sup>, Jingyao Wang<sup>1,2</sup>, Wenwen Qiang<sup>1,2\*</sup>,

<sup>1</sup>University of Chinese Academy of Sciences, <sup>2</sup>Institute of Software Chinese Academy of Sciences

## Abstract

Self-supervised contrastive learning (SSCL) has recently demonstrated superiority in multiple downstream tasks. In this paper, we generalize the standard SSCL methods to a **Generalized Learning Framework (GLF)** consisting of two parts: the aligning part and the constraining part. We analyze three existing SSCL methods: BYOL, Barlow Twins, and SwAV, and show that they can be unified under GLF with different choices of the constraining part. We further propose empirical and theoretical analyses providing two insights into designing the constraining part of GLF: intra-class compactness and inter-class separability, which measure how well the feature space preserves the class information of the inputs. However, since SSCL can not use labels, it is challenging to design a constraining part that satisfies these properties. To address this issue, we consider inducing intra-class compactness and inter-class separability by iteratively capturing the dynamic relationship between anchor and other samples and propose a plug-and-play method called **Adaptive Distribution Calibration (ADC)** to ensure that samples that are near or far from the anchor point in the original input space are closer or further away from the anchor point in the feature space. Both the theoretical analysis and the empirical evaluation demonstrate the superiority of ADC.

## Introduction

Representation learning without pairwise constraints is a high-profile research concern in the field of machine learning. Contrastive learning (CL), as an innovative self-supervised contrastive learning (SSCL) approach, has recently demonstrated superiority in various tasks, e.g., classification, object detection, and segmentation (Jaiswal et al. 2020; Si et al. 2022; Wang et al. 2023; Radford et al. 2021b; Wang et al. 2024). A characteristic of CL is its instance-based learning paradigm. That is, CL considers each sample in the training dataset as a separate class. Based on such a simple but graceful paradigm, CL can learn semantic information from the data itself, which can be delivered to various downstream tasks with satisfactory performance. As CL continues to develop, state-of-the-art methods such as SimCLR (Chen et al. 2020a) and BYOL (Grill et al. 2020b) are narrowing the performance gap with supervised methods.

In general, CL learns the feature extractor by minimizing the contrastive loss. (Wang and Isola 2020) decomposed

the contrastive loss into two parts: alignment and uniformity. Alignment aims to constrain the similarity between positive samples and anchors, while uniformity aims to constrain the distribution of all samples to satisfy a uniform distribution. (Chen, Luo, and Li 2021) provided a closer analysis of uniformity and suggested that it is also valid to constrain the distribution of all samples to satisfy other distributions, such as Gaussian or high-dimensional uniform distributions. Among these methods, the first term in their objective can be interpreted as aligning, while the second term is considered as constraining the data distribution to satisfy a definitive condition. From this perspective, we generalize the standard self-supervised contrastive learning (SSCL) method and propose a **Generalized Learning Framework (GLF)**. Specifically, it consists of two parts: the aligning part and the constraining part. The aligning part aims to align two augmented samples with the same ancestor in the feature space, while the constraining part imposes a priori constraints on the training data. GLF is generalized in the sense that its constraining part can be any reasonable form of constraints, not limited to distributional constraints.

One question that arises is what kind of constraining part can be beneficial for improving the performance of contrastive learning in downstream tasks. We answer this question from two aspects. The first aspect is empirical analysis (**Subsection “Empirical Analysis”**). In brief, we provide an empirical analysis of four representative SSCL methods and conclude that their objective functions do not model the dynamic relationship between augmented samples. As a result, they all face the problem of insufficient separability of data distributions of different categories. We verify this by running toy experiments on four benchmark datasets with five different constraints, which further indicate that if the constraints under the new framework can make points from different categories move away from each other, it can significantly improve the performance of SSCL methods. The second aspect is theoretical analysis (**Subsection “Theoretical Analysis”**). We further demonstrate that if the constraining part under the new framework can make points of the same category in the feature space cluster with each other, it can significantly improve the performance of SSCL methods. These two aspects provide insights into the design of the constraining part under the new framework. An ideal constraining part should make points of the same class cluster

\*Corresponding author.

together as much as possible while keeping points of different classes as far apart as possible.

Guided by the above insights, we propose a new constraining part under GLF called **Adaptive Distribution Calibration (ADC)**. ADC can be viewed as a learnable regularization term that can be directly integrated into existing SSCL models. The core idea of ADC is to iteratively treat the samples in the dataset as anchors and control other samples to aggregate or move away from anchors according to the similarity between samples. This induces the effect of aggregating samples with the same classes and separating samples with dissimilar classes. ADC consists of two parts: the Distribution Calibration Module (DCM) and the Local Preserving Module (LPM). DCM aims to aggregate similar samples together and separate dissimilar samples from each other through learnable distribution calibration. Specifically, DCM assumes that there are two distributions in the feature space: a calibration distribution which is set as a multivariate Gaussian distribution, and a data distribution which is set as a multivariate  $t$ -distribution. By minimizing the KL-divergence between these two distributions, samples in the feature space can be automatically aggregated or separated. However, the poor performance of the feature extractor at the early stage of training may cause the distance of the samples in the feature space from the anchor point to change, which in turn causes the DCM to aggregate or separate the samples incorrectly. Meanwhile, when outliers are selected as anchor, DCM will cause some samples in the dataset to cluster towards outliers, resulting in wrong clustering among samples. To alleviate these problems, LPM proposes to constrain the positions of samples in the feature space to be consistent with their positions in the original space using a Dirichlet distribution (DD). Also, LPM uses an interesting observation of DD to mitigate the effects of outliers. Our major contributions are as follows:

- We develop a generalized learning framework (GLF) that extends the standard SSL approach. GLF consists of two components: an aligning part and a constraining part.
- Based on the empirical and theoretical analyses, we find that an ideal constraint should maximize the clustering of points belonging to the same class while keeping points from different classes as far apart as possible.
- We propose a plug-and-play method that can be integrated into existing models. The core concept is to ensure points that are close or far away in the original input space are closer or farther away in the feature space.
- We provide a theoretical guarantee on the error bound for the classification task and conduct empirical evaluations to demonstrate that our proposed method can improve the performance of various state-of-the-art SSCL methods.

## Related Work

Contrastive learning (CL) has been well studied as a high-profile approach to learning visual representations without labels (Oord, Li, and Vinyals 2018; Tian, Krishnan, and Isola 2020a; Hjelm et al. 2018). SimCLR (Chen et al. 2020a) is the first widely used contrastive learning method that significantly narrows the gap with supervised learning. However,

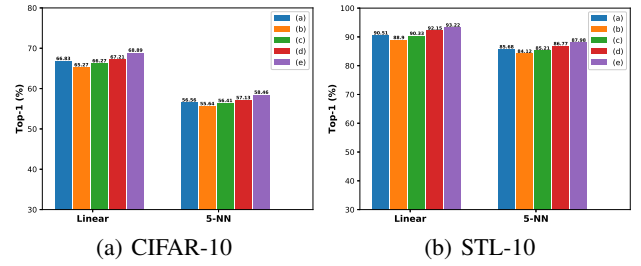


Figure 1: Motivating Example. We have experimented with five different approaches on two benchmark datasets. Different colors indicate the comparison learning models obtained by training based on different prior distributions.

SimCLR requires large training batches and, thus, high computational resource requirements. Then, MoCo (He et al. 2020; Chen et al. 2020b; Chen, Xie, and He 2021) is proposed to mitigate this problem by dynamic memory allocation. MetAug (Li et al. 2022) proposes an augmentation generation mechanism to generate hard positive samples to alleviate the problem of too many negative samples. Also, some methods propose to alleviate this problem by using a no-negative-sample strategy, e.g., BYOL (Grill et al. 2020a), W-MSE (Ermolov et al. 2021), Simsiam (Chen and He 2021), and Barlow Twins (Zbontar et al. 2021). A problem among these methods is that the intrinsic structure of the data distribution is ignored. To solve this problem, SwAV (Caron et al. 2020) and PCL (Li et al. 2020) propose to excavate the clustering structures embedded in data distribution. LMCL (Chen et al. 2021) proposes to mine the large margin between the positive samples and the negative samples related to the anchor. Contrastive learning can be viewed as an instance-based learning paradigm. Thus, the related methods can not explore the relationship between different instances. Based on this problem, ReSSL (Zheng et al. 2021; Tomasev et al. 2022) is proposed to measure the similarity of the data distribution based on two augmented samples. Different from these mentioned methods, the proposed ADC is to induce the clustering structures in an instance-based manner. We aim to constrain points closer to the anchor in the original space to be closer to the feature space and points farther from the anchor to be farther away in the feature space.

## Problem Formulation and Analysis

In this section, we present an overview of SimCLR (Chen et al. 2020a) for the alignment and uniformity properties and propose a generalized framework by considering the uniformity of SimCLR as a constraint on the training data. We then revisit three representative SSCL methods within this framework. Furthermore, we provide insights into SSCL through both theoretical and empirical analysis.

Given a mini-batch of training data  $X_{tr} = \{x_i\}_{i=1}^N$ , where  $x_i$  denotes the  $i$ -th sample and  $N$  represents the number of samples, we generate an augmented dataset  $X_{tr}^{aug} = \{x_1^1, x_1^2, \dots, x_N^1, x_N^2\}$  by applying stochastic data augmentation (e.g., random crop) to transform each sample  $x_i$

into two augmented views  $x_i^1$  and  $x_i^2$ . We can also obtain  $X_{tr}^{aug} = \{X_{tr}^{aug,1}, X_{tr}^{aug,2}\}$ , where  $X_{tr}^{aug,i} = \{x_1^i, \dots, x_N^i\}$  and  $i \in \{1, 2\}$ . The samples in  $X_{tr}$  are considered as ancestors of those in  $X_{tr}^{aug}$ . SSCL (Chen et al. 2020a; Wang and Isola 2020) involves training a feature extractor  $f$  to project input samples from their original space  $\mathcal{X}$  into a feature space  $\mathcal{Z}$ , thus we have:  $z_i^j = f(x_i^j)$ , where  $i \in \{1, 2, \dots, N\}$  and  $j \in \{1, 2\}$ . The goal of SSCL is to learn a general representation that is suitable for downstream tasks.

## Overview of SimCLR

SimCLR (Chen et al. 2020a) is an instance-based learning method that treats each sample as a separate class during training. It minimizes the contrastive loss in the feature space to bring points of the same class closer together while separating points of different classes. The objective is:

$$\mathcal{L}_{NCE} = \sum_{i=1, l=1}^{i=N, l=2} -\log \frac{\exp\left[\frac{\text{sim}(z_i^l, z_i^{3-l})}{\tau}\right]}{\exp\left[\frac{\text{sim}(z_i^l, z_i^{3-l})}{\tau}\right] + \sum_{j=1, j \neq i, k=1}^{j=N, k=2} \exp\left[\frac{\text{sim}(z_i^l, z_j^k)}{\tau}\right]}, \quad (1)$$

where  $\tau$  represents the temperature hyperparameter,  $z_i^j = f_p(z_i^j)$ ,  $f_p$  represents the projection head, and  $\text{sim}(x, y) = x^T y / \|x\| \|y\|$  is the  $l_2$ -normalized cosine similarity between  $x$  and  $y$ . According to Theorem 1 in (Wang and Isola 2020), as  $N \rightarrow \infty$ , Equation (1) can be rewritten as:

$$\mathcal{L}_{NCE} = -\frac{1}{\tau} \mathbb{E}_{(z_i, z_j) \sim p_{pos}} \text{sim}(z_i, z_j) + \mathbb{E}_{z^i \sim p_{data}} \left[ \log \mathbb{E}_{z^j \sim p_{data}} \exp\left(\frac{\text{sim}(z^i, z^j)}{\tau}\right) \right], \quad (2)$$

where  $p_{pos}$  represents the distribution of positive pairs and  $p_{data}$  represents the data distribution. Then, based on the von Mises-Fisher (vMF) kernel density estimation (KDE) (Cohn and Kumar 2007; Borodachov, Hardin, and Saff 2019), the second term in Equation (2) can be considered:

$$\begin{aligned} & \mathbb{E}_{x \sim p_{data}} \left[ \log \mathbb{E}_{x^- \sim p_{data}} \left[ e^{-F(x)^T F(x^-) / \tau} \right] \right] \\ &= \frac{1}{N} \sum_{i=1}^N \log p_{\text{vMF-KDE}}(F(x_i)) + \log Z_{\text{vMF}} \triangleq -H(F(x)), \end{aligned} \quad (3)$$

where  $F(x) = f_p(f(x))$ ,  $p_{\text{vMF-KDE}}$  is the KDE-based vMF kernel with  $\kappa = \tau^{-1}$ ,  $Z_{\text{vMF}}$  is the vMF normalization constant for  $\kappa = \tau^{-1}$ , and  $H(\cdot)$  is the entropy estimator.

## Generalized Learning Framework of SSCL

In Eq.(2), the first term can be interpreted as aligning, while the second term is considered as constraining the data distribution to be uniform. From this perspective, we generalize the standard self-supervised contrastive learning (SSCL) method to a generalized learning framework (GLF).

Specifically, the proposed GLF consists of two parts: the aligning part  $\mathcal{L}_{\text{align}}$  and the constraining part  $\mathcal{L}_{\text{constrain}}$ . The aligning part aims to align the two augmented samples with the same ancestor in the feature space, while the constraining part imposes a priori constraints on the training data. Thus, the objective function of GLF can be expressed as:

$$\min_{f, f_p} \mathcal{L}_{\text{align}}(X_{tr}^{aug}, f, f_p) + \mathcal{L}_{\text{constrain}}(X_{tr}^{aug}, f, f_p). \quad (4)$$

## Empirical Analysis

In this section, we empirically analyze four representative SSCL methods—SimCLR (Chen et al. 2020a), BYOL (Grill et al. 2020a), Barlow Twins (Zbontar et al. 2021), and SwAV (Caron et al. 2020)—and examine the design implications for constraint components within our proposed framework.

In SimCLR, the second term of Eq.(2) promotes a uniform distribution over augmented samples, encouraging them to span the feature space. However, this often leads to distributional overlap near the feature boundaries, reducing class separability and feature discriminability. BYOL’s objective in Eq.(20) constrains only the parameter update dynamics, without explicitly modeling positional relationships among augmented views. Barlow Twins (Eq.(23)) minimizes feature redundancy across dimensions but ignores inter-sample relationships in the embedding space. SwAV (Eq.(26)) introduces clustering to align augmented views but lacks mechanisms to enforce inter-class separation. Ideally, discriminative features should exhibit clear structure: samples from the same class should cluster tightly, while those from different classes should remain well-separated. However, the above methods do not explicitly model relationships among samples with different ancestors, resulting in limited inter-class separability in the feature space.

To address this, we argue that effective constraints should explicitly encourage inter-class separation to enhance feature discriminability. We validate this claim through toy experiments on two benchmark datasets using five constraint designs: (a) enforcing a uniform hyperspherical distribution, (b) enforcing a uniform hypercube distribution, (c) enforcing a Gaussian distribution with batch-wise empirical mean and covariance, (d) enforcing a Gaussian distribution with batch-wise empirical mean and identity covariance, (e) modeling a mixture of Gaussians by clustering each mini-batch using DBSCAN (Ram et al. 2010), computing cluster-wise means, and constructing isotropic Gaussians per cluster. Figure 1 shows that (e) yields the best performance, suggesting that encouraging separation between samples from different categories significantly improves performance.

## Theoretical Analysis

In this subsection, we analyze the contrastive learning method from a theoretical perspective and provide another insight for designing the constraining part. Given an anchor  $x$ , denote  $x^+$  as the positive sample,  $p(x, x^+)$  as the joint distribution of  $x, x^+$ , and  $y \in \{1, \dots, K\}$  as the label. Let  $p(y)$  be the class probability distribution and  $p_y(x)$  be the data probability distribution over class  $y$ . We assume positive samples are sampled from the same data distribution as an anchor and negative samples are sampled based on the probability distribution  $\mathbb{E}_{y \sim p(y)} p_y(x)$ .

We assume that the labels between  $x$  and  $x^+$  are deterministic and consistent, e.g.,  $p(y|x) = p(y|x^+)$ . We consider the mean CE loss, which is denoted as:

$$\mathcal{L}_{CE}^\mu(f) = \mathbb{E}_{p(x, y)} \left[ -\log \frac{\exp(f(x)^T \mu_y)}{\sum_{i=1}^K \exp(f(x)^T \mu_i)} \right], \quad (5)$$

where  $\mu_i = \mathbb{E}_{(x|y=i)}[f(x)]$  is the class mean vector. From (Arora et al. 2019), we obtain  $\mathcal{L}_{CE}^\mu(f)$  upper bounds the standard cross entropy loss, e.g.,  $\mathcal{L}_{CE}^\mu(f) \geq \min_{g_c} \mathcal{L}_{CE}(f, g_c)$ , where  $g_c$  is the classifier. Then, let  $S = \{x_j, x_j^+, x_{j,1}^-, \dots, x_{j,n}^-\}_{j=1}^M$  be the training set. We can characterize the generalization gap between contrastive learning and supervised learning risks by the following Theorem.

**Theorem 1.** *Let  $f^* \in \arg \min_{f \in \mathcal{F}} \mathcal{L}_{NCE}$ , where  $\mathcal{F}$  represents the function space. Then with probability at least  $1 - \delta$ , we have:*

$$\mathcal{L}_{CE}^\mu(f^*) \leq \mathcal{L}_{NCE}(f) + \sqrt{\text{Var}(f(x)|y)} + \mathcal{M}(n), \quad (6)$$

where  $n$  is the batch size,  $\mathcal{M}(n)$  can be represented as:

$$\mathcal{M}(n) = \mathcal{O}\left(n^{-1/2}\right) - \log \frac{n}{K} + \mathcal{O}\left(\frac{\sqrt{1+1/n} \mathfrak{R}_{\mathcal{F}}(\zeta)}{M} + \sqrt{\frac{\log(1/\delta) \log^2(n)}{M}}\right), \quad (7)$$

where the Rademacher complexity  $\mathfrak{R}_{\mathcal{F}}(\zeta)$  is denoted as  $\mathfrak{R}_{\mathcal{F}}(\zeta) = E_{\zeta \sim \{\pm 1\}^{(n+2)Md}} [\sup_{f \in \mathcal{F}} \langle \zeta, F \rangle]$ ,  $d$  is the output dimension of the  $f$  and  $F \in R^{(n+2)Md}$  can be represented as  $F = (f_t(x_j), f_t(x_j^+), f_t(x_{j,1}^-), \dots, f_t(x_{j,n}^-))_{j \in [M], t \in [d]}$ .

From Theorem 1, we observe that when  $\text{Var}(f(x)|y)$  equals to 0, the  $\mathcal{L}_{CE}^\mu(f^*)$  is only bounded by  $\mathcal{L}_{NCE}(f)$ . Therefore, minimizing  $\text{Var}(f(x)|y)$  is conducive to improving the performance of learned  $f^*$  in downstream tasks. This further indicates that if the constraining part under the new framework can make the points of the same category in the feature space cluster with each other, it can significantly improve the performance of SSCL methods.

## Methodology

Based on the above results, an ideal constraint should encourage tight clustering of same-class samples while separating those from different classes. However, without label information, class membership remains unknown during training. To address this, we propose an anchor-based strategy (**Figure 2**), called Adaptive Distribution Calibration (ADC): each training sample is treated as an anchor, and we enforce that samples nearby in the input space stay close in the feature space, while more distant samples are pushed further apart. This process is applied iteratively across the training set. In the absence of severe outliers, this approximation promotes intra-class compactness and inter-class separability. It comprises two key components: a distribution calibration module and a local structure preservation module. Since existing SSCL methods already include an alignment objective, ADC can be used as a plug-and-play constraint module compatible with standard SSCL frameworks.

## The Proposed Method

**Distribution Calibration Module** The Distribution Calibration Module (DCM) dynamically induces aggregation or separation among samples in the feature space. Given an anchor, DCM attracts certain samples toward the anchor while repelling others away, thereby calibrating their relative positions. This anchor-based mechanism adjusts local feature

geometry in a data-driven manner. Formally, let  $p_{\text{data}}$  denote the training data distribution, and let  $x_i \sim p_{\text{data}}$  be a sampled instance with feature representation  $z_i = f(x_i)$ . We treat  $x_i$  as the anchor and apply a projection head  $f_p(\cdot)$ , yielding  $z_i = f_p(z_i)$ . The calibration distribution is modeled as a multivariate Gaussian  $\mathcal{N}(z; z_i, \Sigma)$ , centered at  $z_i$  with covariance  $\Sigma$ , estimated from the training data. Meanwhile, the data distribution is approximated by a multivariate Student's  $t$ -distribution  $\mathcal{F}(z; z_i, \Sigma')$ , with the same mean and a scaled covariance  $\Sigma' = \rho \Sigma / (\rho - 2)$ , where  $\rho > 2$  controls the heavy-tailedness. We then define:

$$\mathcal{N}(z; z_i, \Sigma) = \frac{\exp\{\frac{1}{2}[z - z_i]^T \Sigma^{-1}[z - z_i]\}}{\sqrt{(2\pi)^k \det(\Sigma)}}, \quad (8)$$

where  $k$  is the dimension of  $z_i$ . Meanwhile, we have:

$$\mathcal{F}(z; z_i, \Sigma') = \frac{\Gamma(\frac{\rho+k}{2}) \{1 + [(z - z_i)^T \Sigma'^{-1}(z - z_i)]\}^{-\frac{\rho+k}{2}}}{\Gamma(\frac{\rho}{2}) \rho^{\frac{\rho}{2}} \pi^{\frac{\rho}{2}} \det(\Sigma')^{\frac{1}{2}}}, \quad (9)$$

where  $\Gamma(\cdot)$  denotes the gamma function. To encourage similar samples to cluster around the anchor while pushing dissimilar samples away in the feature space, we define the objective of DCM as:

$$\mathcal{L}_{DCM} = \sum_i \text{KL}(\text{Sg}(\mathcal{N}(z; z_i, \Sigma)) | \mathcal{F}(z; z_i, \Sigma')), \quad (10)$$

where  $\text{KL}(\cdot)$  denotes the Kullback–Leibler divergence, and  $\text{Sg}(\cdot)$  is the stop-gradient operator, which prevents gradients from backpropagating through its input. Given  $z_i$  and  $\Sigma$ , the multivariate Gaussian distribution has a higher probability density than the multivariate  $t$ -distribution near the mean (i.e., in the head region), but a lower density in the tails (i.e., regions far from the mean) (Ferguson 1962; Molenberghs and Lesaffre 1997; Van der Maaten and Hinton 2008). This behavior is illustrated in **Figure 3**. Assuming  $z_j^1$  lies close to  $z_j$  and  $z_j^2$  lies farther away, we derive the following  $\mathcal{N}(z_j^1; z_i, \Sigma) > \mathcal{F}(z_j^1; z_i, \Sigma')$  and  $\mathcal{N}(z_j^2; z_i, \Sigma) < \mathcal{F}(z_j^2; z_i, \Sigma')$ . Then, minimizing **Eq.(10)** can be thought of as constraining  $\mathcal{N}(z_j^1; z_i, \Sigma) = \mathcal{F}(z_j^1; z_i, \Sigma')$  and  $\mathcal{N}(z_j^2; z_i, \Sigma) = \mathcal{F}(z_j^2; z_i, \Sigma')$ . If the density value of each sample in  $\mathcal{N}(\cdot; z_i, \Sigma)$  is fixed, the way for minimizing **Eq.(10)** is to restrict  $z_j^1$  and  $z_i$  to be closer together while  $z_j^2$  and  $z_i$  are farther apart in the feature space, thus leading to larger  $\mathcal{F}(z_j^1; z_i, \Sigma')$  and smaller  $\mathcal{F}(z_j^2; z_i, \Sigma')$ .

Empirically, given a mini-batch of training data  $X = \{x_1, \dots, x_n\}$  with batch size  $n$ , we input them into functions  $f$  and  $f_p$  to obtain  $Z = \{z_1, \dots, z_n\}$ . Using  $z_i$  as the anchor, we present the discretized forms of  $\mathcal{N}(z_j; z_i, \Sigma)$  and  $\mathcal{F}(z_j; z_i, \Sigma')$  respectively. For  $z_j \in Z$ , the calibration distribution values  $p_{\text{cal}}^i$  and data distribution values  $p_{\text{dat}}^i$  is:

$$p_{\text{cal}}^i(z_j) = \frac{\mathcal{N}(z_j; z_i, \Sigma)}{\sum_{j=1}^n \mathcal{N}(z_j; z_i, \Sigma)}, p_{\text{dat}}^i(z_j) = \frac{\mathcal{F}(z_j; z_i, \Sigma')}{\sum_{j=1}^n \mathcal{F}(z_j; z_i, \Sigma')}. \quad (11)$$

Therefore, **Eq.(10)** can be rewritten as:

$$\mathcal{L}_{DCM} = \sum_{i=1}^n \sum_{j=1}^{n-1} \text{Sg}(p_{\text{cal}}^i(z_j)) \log \frac{\text{Sg}(p_{\text{cal}}^i(z_j))}{p_{\text{dat}}^i(z_j)}. \quad (12)$$

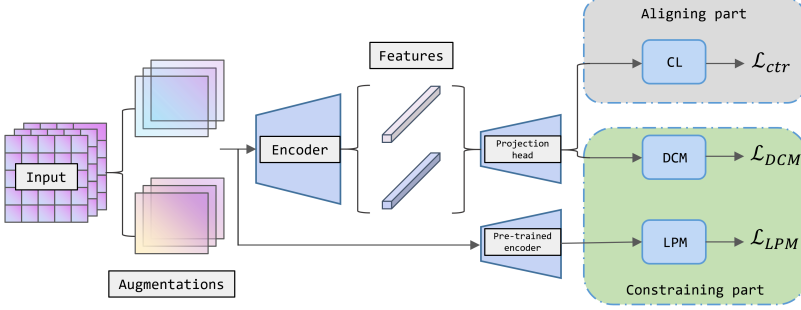


Figure 2: The overall pipeline of the proposed ADC. It consists of two parts: the aligning part and the constraining part.

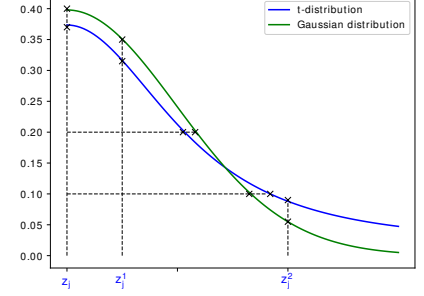


Figure 3: Visualization of the Gaussian distribution and the  $t$ -distribution.

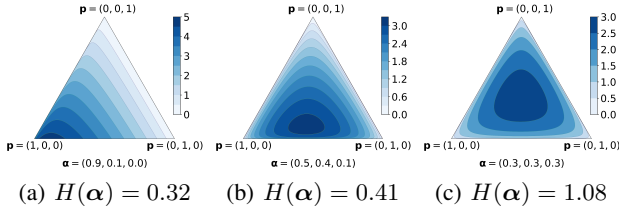


Figure 4: The visualizations of three kinds of DD.

By minimizing **Eq.(12)**, samples with high probability density (i.e., close to the anchor in feature space) are pulled closer to the anchor, while those with low density (i.e., farther from the anchor) are pushed away. As nearby samples are more likely to belong to the same class, iterating over the entire training set and treating each sample as an anchor enables approximate distribution calibration, promoting intra-class compactness and inter-class separability.

**Local Preserving Module** DCM operates in the feature space by measuring distances between augmented samples, but its effectiveness may be compromised during early training when the feature extractor is under-optimized. In this phase, samples that are close or distant in the input space may be misrepresented in the feature space. Moreover, if an outlier is chosen as the anchor, DCM may erroneously attract surrounding samples, leading to distorted representations. To address these issues, we introduce a Local Preservation Module (LPM) that enforces local consistency by preserving relative input-space distances in the feature space. LPM also quantifies the likelihood of an anchor being an outlier using information entropy and down-weights its influence through an adaptive weighting scheme. Before presenting DCM in detail, we first introduce the Dirichlet Distribution (DD) (Ng, Tian, and Tang 2011).

**Definition 1. (Dirichlet Distribution)** The Dirichlet distribution of order  $K \geq 2$  with parameters  $\alpha_1, \dots, \alpha_K \geq 0$  has a probability density function with respect to Lebesgue measure on the Euclidean space  $\mathbb{R}^{K-1}$ , which can be given by

$$\text{Dir}(\beta|\alpha) = \begin{cases} \frac{1}{B(\alpha)} \prod_{i=1}^K \beta_i^{\alpha_i-1}, & \text{for } \beta \in S_K \\ 0, & \text{otherwise,} \end{cases} \quad (13)$$

where  $\alpha = [\alpha_1, \dots, \alpha_K]$ ,  $\beta = [\beta_1, \dots, \beta_K]$ , and  $S_K$  belong to the standard  $k-1$  simplex, or in other words  $S_K = \left\{ \beta \mid \sum_{i=1}^K \beta_i = 1 \text{ and } 0 \leq \beta_1, \dots, \beta_K \leq 1 \right\}$ . The normalizing constant is the multivariate beta function, which can be expressed in terms of the gamma function  $B(\alpha) = \frac{\prod_{i=1}^K \Gamma(\alpha_i)}{\Gamma(\sum_{i=1}^K \alpha_i)}$ , where  $\Gamma(\cdot)$  is the gamma function.

According to **Eq.(13)**, the expectation of DD is:

$$\mathbb{E}_{\text{Dir}(\beta|\alpha)}(\beta) = \alpha / \sum_{i=1}^K \alpha_i. \quad (14)$$

We have  $\mathbb{E}_{\text{Dir}(\beta|\alpha)}(\beta) = \alpha$  when  $\sum_{i=1}^K \alpha_i = 1$ . Based on Definition 1, the probability density of  $\text{Dir}(\beta|\alpha)$  is high when  $\beta$  is close to  $\alpha$ , and low otherwise. As illustrated in Figure 4, the Dirichlet distribution exhibits an aggregation behavior: when  $\sum_{i=1}^K \alpha_i = 1$ , a smaller entropy  $H(\alpha)$  leads to a sharper concentration of the probability density near  $\alpha$ , while a larger entropy flattens the density surface, spreading probability mass more evenly across the domain.

The Local Preservation Module (LPM) is derived from this property of the Dirichlet distribution. Given a mini-batch of training data  $X = \{x_1, \dots, x_n\}$  with corresponding feature representations  $Z = \{z_1, \dots, z_n\}$  computed by functions  $f$  and  $f_p$ , we use a CLIP-pretrained feature extractor  $f_{\text{pre}}$  (Radford et al. 2021a) to obtain prior representations  $Z^{\text{pre}} = \{z_1^{\text{pre}}, \dots, z_n^{\text{pre}}\}$ . Treating  $x_i$  as the anchor, its prior representation is  $z_i^{\text{pre}}$ , and the corresponding multivariate  $t$ -distribution is denoted  $\mathcal{F}(z_i^{\text{pre}}; z_i^{\text{pre}}, \Sigma')$ . The normalized, discretized form of this distribution is given by:

$$p_{\text{pre}}^i(z_j^{\text{pre}}) = \frac{\mathcal{F}(z_j^{\text{pre}}; z_i^{\text{pre}}, \Sigma')}{\sum_{j=1}^n \mathcal{F}(z_j^{\text{pre}}; z_i^{\text{pre}}, \Sigma')}, \forall z_j^{\text{pre}} \in Z^{\text{pre}}. \quad (15)$$

We define  $\mathbb{P}_{\text{data}}^i = \{p_{\text{data}}^i(z_j)\}_{j \neq i}$  and  $\mathbb{P}_{\text{pre}}^i = \{p_{\text{pre}}^i(z_j)\}_{j \neq i}$ , excluding the anchor index  $i$ . Since  $\mathbb{P}_{\text{pre}}^i$  is computed using a pretrained model known for producing semantically meaningful features, distances in  $Z^{\text{pre}}$  better reflect the true

relative positions. Thus, samples closer to the anchor have higher probabilities in  $\mathbb{P}_{\text{pre}}^i$ , and more distant ones have lower values. To preserve this, LPM encourages  $\mathbb{P}_{\text{data}}^i$  to lie in the high-density region of  $\text{Dir}(\mathbb{P}_{\text{data}}^i | \mathbb{P}_{\text{pre}}^i)$ , yielding:

$$\mathcal{L}_{LPM} = \sum_{i=1}^n \text{Dir}(\mathbb{P}_i^{\text{data}} | \mathbb{P}_i^{\text{pre}}). \quad (16)$$

Maximizing **Eq. (16)** encourages samples that are close in the input space to remain close in the feature space, while pushing apart those that are distant, thereby mitigating DCM’s miscalibration. We do not enforce  $\mathbb{P}_i^{\text{pre}} = \mathbb{P}_i^{\text{cal}}$  explicitly, as anchors are randomly selected from  $X$ , and the induced multivariate  $t$ -distribution accurately reflects local structure only when the anchor aligns with the true class center. Ideally, samples from the same class would share a common anchor. Optimizing **Eq. (16)** implicitly promotes consistent local topology across anchors or alignment with class centers. Moreover, when an anchor is an outlier, its distances to other samples tend to be uniform, causing  $\mathbb{P}_i^{\text{pre}}$  to approximate a uniform distribution. To reduce the impact of such cases, LPM incorporates a weighted calibration strategy into **Eq. (12)**, leveraging properties of the Dirichlet distribution:

$$\mathcal{L}_{DCM} = \frac{1}{H(\mathbb{P}_i^{\text{pre}})} \sum_{i=1}^n \sum_{j=1}^{n-1} \text{Sg}(p_{\text{cal}}^i(z_j)) \log \frac{\text{Sg}(p_{\text{cat}}^i(z_j))}{p_{\text{dat}}^i(z_j)}. \quad (17)$$

As observed from the properties of the Dirichlet distribution, when the anchor lies within the distribution, the induced  $\mathbb{P}_i^{\text{pre}}$  contains a mix of high and low probabilities, resulting in low entropy  $H(\mathbb{P}_i^{\text{pre}})$ . In contrast, when the anchor is an outlier, the probabilities are nearly uniform, yielding high entropy. Therefore, minimizing **Eq. (17)** effectively reduces the influence of outlier anchors.

## Overall Objective

Finally, given the feature extractor  $f$ , the pre-trained  $f_{\text{pre}}$ , the projection head  $f_p$ , the objective of ADC is:

$$\mathcal{L}(f, f_p) = \mathcal{L}_{\text{ctr}}(f, f_p) + \nu \mathcal{L}_{DCM}(f, f_p) - \nu \mathcal{L}_{LPM}(f, f_p), \quad (18)$$

where  $\nu, \nu > 0$  are temperature hyperparameters, and  $\mathcal{L}_{\text{ctr}}(f, f_p)$  denotes the loss used in SSCL methods. Unlike negative-sample-based methods (NSB-m) such as Hard (Robinson et al. 2020) and Debaised (Chuang et al. 2020), which mitigate false negatives by pulling together augmented views of the same instance, ADC fundamentally differs in its objective. NSB-m methods often ignore relationships between different instances of the same class, resulting in high within-class variance. In contrast, ADC explicitly promotes intra-class compactness by aligning samples from different instances but the same class, while ensuring inter-class separation across distinct ancestors, thereby enhancing both alignment and discrimination.

## Experiments

To evaluate ADC, we conduct extensive experiments on both the benchmark and the real-world datasets, including tasks like classification, object detection, and segmentation (See

Method	CIFAR-10		CIFAR-100		STL-10	
	linear	5-nn	linear	5-nn	linear	5-nn
MoCo	91.69	88.66	67.02	56.29	90.64	88.01
SimSiam	91.71	88.65	67.22	56.36	91.01	88.16
SimCLR	91.80	88.42	66.83	56.56	90.51	85.68
BYOL	91.73	89.45	66.60	56.82	91.99	88.64
Barlow Twins	91.43	89.68	66.13	56.70	90.38	87.13
W-MSE	91.99	89.87	67.64	56.45	91.75	88.59
ReSSL	90.20	88.26	66.79	53.72	88.25	86.33
MEC	90.55	87.80	67.36	57.25	91.33	89.03
VICRegL	90.99	88.75	68.03	57.34	92.12	90.01
SimSiam+DCM	92.21	89.25	67.89	57.56	91.61	88.69
SimCLR+DCM	92.34	89.05	67.52	57.10	91.12	86.51
BYOL+DCM	92.30	90.02	67.20	57.38	92.51	89.51
Barlow Twins+DCM	91.97	90.22	66.83	57.29	91.01	87.77
W-MSE+DCM	92.58	90.39	68.22	57.01	92.27	89.11
VICRegL+DCM	92.00	90.15	68.38	57.32	91.89	89.06
SimSiam+LPM	92.22	89.19	67.91	57.48	91.64	88.72
SimCLR+LPM	92.35	89.11	67.44	57.18	91.21	86.47
BYOL+LPM	92.31	90.01	67.16	57.31	92.53	89.49
Barlow Twins+LPM	91.94	90.21	66.81	57.30	91.09	87.74
W-MSE+LPM	92.54	90.42	68.27	57.11	92.21	89.02
VICRegL+LPM	91.95	90.19	68.42	57.28	91.92	89.01
SimSiam+ADC	93.41	90.62	69.23	58.89	92.86	89.80
SimCLR+ADC	93.46	89.55	68.93	58.51	92.35	88.02
BYOL+ADC	93.70	89.35	68.43	58.72	94.01	90.91
Barlow Twins+ADC	93.19	90.32	68.24	58.62	92.20	89.14
W-MSE+ADC	93.81	91.52	69.57	58.29	93.68	90.43
VICRegL+ADC	92.84	90.52	69.04	59.02	92.18	89.07

Table 1: The classification accuracies of a linear classifier (linear) and a 5-nearest neighbors classifier (5-nn) with a ResNet-18. Full results are shown in **Table 6**.

**Appendices** for details and full results). All experiments are the average of five runs on NVIDIA V100 GPUs.

## Comprison and Evaluation

**Benchmark Dataset** We select on eight benchmark datasets, including CIFAR-10 (Krizhevsky, Hinton et al. 2009), CIFAR-100 (Krizhevsky, Hinton et al. 2009), STL-10 (Coates, Ng, and Lee 2011), Tiny ImageNet (Le and Yang 2015), ImageNet-100 (Tian, Krishnan, and Isola 2020b), ImageNet (Krizhevsky, Sutskever, and Hinton 2012), PASCAL VOC (Everingham et al. 2010), and COCO (Lin et al. 2014). For real-world data, we deploy a radar- and camera-based workstation near the coast of Sanya, operating continuously to monitor offshore regions and capture large volumes of ship imagery. The collected raw data is then processed into two structured datasets. **Full results and details are provided in Appendix due to space limitation.**

**Unsupervised learning** Following (Chen et al. 2020a), we freeze the pretrained encoder and train a supervised linear classifier on top. The classifier is optimized using SGD (momentum 0.9, weight decay  $5 \times 10^{-6}$ ) for 500 epochs with a learning rate decaying from  $10^{-2}$  to  $10^{-6}$ . **Table 1** shows that our ADC-based methods consistently outperform exist-



Method	CIFAR-100				ImageNet			
	$f_{pre}^I$	$f_{pre}^{SimCLR}$	$f_{pre}^{CLIP}$	$f_{pre}^{EVA-02}$	$f_{pre}^I$	$f_{pre}^{SimCLR}$	$f_{pre}^{CLIP}$	$f_{pre}^{EVA-02}$
SimCLR + ADC	68.94	68.93	68.93	68.92	73.21	73.22	77.12	77.12
BYOL + ADC	68.43	68.45	68.43	68.44	77.12	77.13	77.12	77.12
Barlow Twins + ADC	68.24	68.23	68.24	68.25	76.05	76.03	76.03	76.04

Table 2: The comparison results using CIFAR-100 and ImageNet across different baselines and pre-trained models.

Method	VOC 07		COCO	
	AP <sub>50</sub>	AP	AP <sub>50</sub> <sup>mask</sup>	AP <sup>mask</sup>
Supervised	74.4	42.4	54.7	33.3
SimCLR	75.9	46.8	54.6	33.3
MoCo	77.1	46.8	55.8	34.4
SimSiam	77.3	48.5	56.0	34.4
MEC	77.4	48.3	56.3	34.7
RELIC v2	76.9	48.0	56.0	34.6
CorInfoMax	76.8	47.6	56.2	34.8
VICRegL	75.9	47.4	56.5	35.1
SimCLR + ADC	77.5	49.0	56.3	35.5
MoCo + ADC	79.0	<b>50.3</b>	57.6	36.0
SimSiam + ADC	<b>79.0</b>	50.3	57.6	35.9
MEC + ADC	78.9	50.2	<b>57.9</b>	<b>36.1</b>
VICRegL + ADC	78.0	49.3	56.6	36.3

Table 3: Transfer learning results on VOC 07 detection and COCO instance segmentation using C4-backbone.

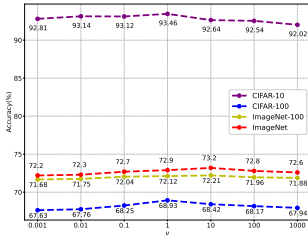


Figure 5: Evaluation on  $\nu$ .

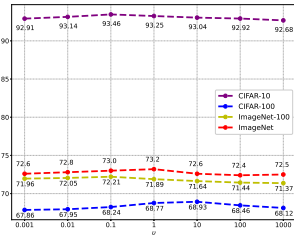


Figure 6: Evaluation on  $v$ .

ing baselines. **Table 6** presents top-1 and top-5 accuracy on ImageNet-100 using ResNet-50, also demonstrating advantages. More results are shown in **Appendix**.

**Semi-supervised learning** We fine-tune models on 1% and 10% subsets of ImageNet labels. Spatial augmentations are applied during training, and standard resizing, cropping, and normalization are used during testing. **Table 8** shows that ADC consistently improves top-1 and top-5 accuracy across both settings, improving by more than 3.5%.

**Transfer learning** Following (Chen et al. 2020a; Liu et al. 2022), we evaluate on object detection and instance segmentation using PASCAL VOC and COCO datasets. We adopt Faster R-CNN with a C4 backbone for VOC and Mask R-CNN for COCO, using Detectron2 settings with learning rate search. **Table 3** shows that SSL methods generally match or exceed supervised baselines, and achieve the best

performance across all tasks with ADC.

**Evaluation on real-world application** We conduct experiments on the Real Ship Classification Dataset (RSCD) and the Real Ship Detection Dataset (RSDD), which includes 10 classes, e.g., cargo ships, fishing boats, sailboats, yachts, etc. The collected images cover diverse scenarios, including challenging conditions, e.g., strong reflections, occlusions, and small targets. **Figure 8**, **Table 10**, and **Table 11** demonstrate that ADC consistently achieves best results.

### Ablation study

We conduct multiple ablation studies and analyses, e.g., the two modules of ADC, feature extractor, hyperparameters, ADC under supervised setting, robustness to outliers, and feature visualization (see Appendix for full results).

**Influence of the proposed two modules.** By setting  $v = 0$  and  $\nu = 0$ , we remove the influence of LPM and DCM. The results in **Tables 1, 7, and 4** show that while DCM and LPM individually outperform baselines, the full ADC model achieves significantly better performance.

**Influence of the pre-trained feature extractor** We select multiple pre-trained settings: (i) an identity matrix  $f_{pre}^I$  for direct similarity computation, (ii) SimCLR pretrained on ImageNet ( $f_{pre}^{SimCLR}$ ), (iii) the CLIP visual encoder ( $f_{pre}^{CLIP}$ ) (Radford et al. 2021a), and (iv) the EVA-02 visual encoder ( $f_{pre}^{EVA-02}$ ) (Fang et al. 2023). **Table 2** shows that ADC is robust to the choice of pre-trained models.

**Parameter Sensitivity** We investigate the influence of hyperparameters in ADC, i.e.,  $\nu$  and  $v$ , with the range of  $\{10^{-3}, 10^{-2}, 10^{-1}, 1, 10, 10^2, 10^3\}$  on multiple benchmark datasets. **Figures 5 and 6** show that the optimal setting for different datasets and demonstrate its stability in practice.

### Conclusion

In this paper, we propose a Generalized Learning Framework (GLF) for SSCL, which has shown impressive performance on various downstream tasks. GLF consists of an aligning component that encourages positive pairs to have similar representations, and a constraining component that imposes additional regularization on the feature space. We analyze representative SSCL methods under GLF based on quantitative measures of their aligning and constraining effects. Based on our analysis, we identify two desirable properties of the constraining component: it should maximize the intra-class compactness and inter-class separability of the

features. To achieve these properties, we introduce a plug-and-play method, which adapts the feature distribution to match the input distribution. Extensive theoretical and empirical results demonstrate that ADC achieves stable improvement on both benchmarks and real-world data.

## References

- Arora, S.; Khandeparkar, H.; Khodak, M.; Plevrakis, O.; and Saunshi, N. 2019. A theoretical analysis of contrastive unsupervised representation learning. *arXiv preprint arXiv:1902.09229*.
- Borodachov, S. V.; Hardin, D. P.; and Saff, E. B. 2019. *Discrete energy on rectifiable sets*. Springer.
- Caron, M.; Misra, I.; Mairal, J.; Goyal, P.; Bojanowski, P.; and Joulin, A. 2020. Unsupervised Learning of Visual Features by Contrasting Cluster Assignments. *CoRR*, abs/2006.09882.
- Chen, S.; Niu, G.; Gong, C.; Li, J.; Yang, J.; and Sugiyama, M. 2021. Large-margin contrastive learning with distance polarization regularizer. In *International Conference on Machine Learning*, 1673–1683. PMLR.
- Chen, T.; Kornblith, S.; Norouzi, M.; and Hinton, G. 2020a. A simple framework for contrastive learning of visual representations. In *International conference on machine learning*, 1597–1607. PMLR.
- Chen, T.; Luo, C.; and Li, L. 2021. Intriguing properties of contrastive losses. *Advances in Neural Information Processing Systems*, 34: 11834–11845.
- Chen, X.; Fan, H.; Girshick, R.; and He, K. 2020b. Improved baselines with momentum contrastive learning. *arXiv preprint arXiv:2003.04297*.
- Chen, X.; and He, K. 2021. Exploring simple siamese representation learning. In *Proceedings of the IEEE/CVF Conference on Computer Vision and Pattern Recognition*, 15750–15758.
- Chen, X.; Xie, S.; and He, K. 2021. An empirical study of training self-supervised vision transformers. In *Proceedings of the IEEE/CVF International Conference on Computer Vision*, 9640–9649.
- Chuang, C.-Y.; Robinson, J.; Lin, Y.-C.; Torralba, A.; and Jegelka, S. 2020. Debaised contrastive learning. *Advances in neural information processing systems*, 33: 8765–8775.
- Coates, A.; Ng, A.; and Lee, H. 2011. An analysis of single-layer networks in unsupervised feature learning. In *Proceedings of the fourteenth international conference on artificial intelligence and statistics*, 215–223. JMLR Workshop and Conference Proceedings.
- Cohn, H.; and Kumar, A. 2007. Universally optimal distribution of points on spheres. *Journal of the American Mathematical Society*, 20(1): 99–148.
- Ermolov, A.; Siarohin, A.; Sangineto, E.; and Sebe, N. 2021. Whitening for self-supervised representation learning. In *International Conference on Machine Learning*, 3015–3024. PMLR.
- Everingham, M.; Van Gool, L.; Williams, C. K.; Winn, J.; and Zisserman, A. 2010. The pascal visual object classes (voc) challenge. *International journal of computer vision*, 88(2): 303–338.
- Fang, Y.; Sun, Q.; Wang, X.; Huang, T.; Wang, X.; and Cao, Y. 2023. EVA-02: A Visual Representation for Neon Genesis. *CoRR*, abs/2303.11331.
- Ferguson, T. S. 1962. A representation of the symmetric bivariate Cauchy distribution. *The Annals of Mathematical Statistics*, 33(4): 1256–1266.
- Grill, J.-B.; Strub, F.; Altché, F.; Tallec, C.; Richemond, P.; Buchatskaya, E.; Doersch, C.; Avila Pires, B.; Guo, Z.; Gheshlaghi Azar, M.; et al. 2020a. Bootstrap your own latent—a new approach to self-supervised learning. *Advances in neural information processing systems*, 33: 21271–21284.
- Grill, J.-B.; Strub, F.; Altché, F.; Tallec, C.; Richemond, P. H.; Buchatskaya, E.; Doersch, C.; Pires, B. A.; Guo, Z. D.; Azar, M. G.; et al. 2020b. Bootstrap your own latent: A new approach to self-supervised learning. *arXiv preprint arXiv:2006.07733*.
- He, K.; Fan, H.; Wu, Y.; Xie, S.; and Girshick, R. 2020. Momentum contrast for unsupervised visual representation learning. In *Proceedings of the IEEE/CVF conference on computer vision and pattern recognition*, 9729–9738.
- Hjelm, R. D.; Fedorov, A.; Lavoie-Marchildon, S.; Grewal, K.; Bachman, P.; Trischler, A.; and Bengio, Y. 2018. Learning deep representations by mutual information estimation and maximization. *arXiv preprint arXiv:1808.06670*.
- Jaiswal, A.; Babu, A. R.; Zadeh, M. Z.; Banerjee, D.; and Makedon, F. 2020. A survey on contrastive self-supervised learning. *Technologies*, 9(1): 2.
- Krizhevsky, A.; Hinton, G.; et al. 2009. Learning multiple layers of features from tiny images.
- Krizhevsky, A.; Sutskever, I.; and Hinton, G. E. 2012. ImageNet classification with deep convolutional neural networks. *Advances in neural information processing systems*, 25: 1097–1105.
- Le, Y.; and Yang, X. 2015. Tiny Imagenet Visual Recognition Challenge. *CS 231N*, 7(7): 3.
- Li, J.; Qiang, W.; Zheng, C.; Su, B.; and Xiong, H. 2022. MetaAug: Contrastive Learning via Meta Feature Augmentation. *International Conference on Machine Learning*.
- Li, J.; Zhou, P.; Xiong, C.; and Hoi, S. C. 2020. Prototypical contrastive learning of unsupervised representations. *arXiv preprint arXiv:2005.04966*.
- Lin, T.-Y.; Maire, M.; Belongie, S.; Hays, J.; Perona, P.; Ramanan, D.; Dollár, P.; and Zitnick, C. L. 2014. Microsoft coco: Common objects in context. In *European conference on computer vision*, 740–755. Springer.
- Liu, X.; Wang, Z.; Li, Y.; and Wang, S. 2022. Self-Supervised Learning via Maximum Entropy Coding. *arXiv preprint arXiv:2210.11464*.
- Molenberghs, G.; and Lesaffre, E. 1997. Non-linear integral equations to approximate bivariate densities with given marginals and dependence function. *Statistica Sinica*, 713–738.
- Ng, K. W.; Tian, G.-L.; and Tang, M.-L. 2011. Dirichlet and related distributions: Theory, methods and applications.



Oord, A. v. d.; Li, Y.; and Vinyals, O. 2018. Representation learning with contrastive predictive coding. *arXiv preprint arXiv:1807.03748*.

Radford, A.; Kim, J. W.; Hallacy, C.; Ramesh, A.; Goh, G.; Agarwal, S.; Sastry, G.; Askell, A.; Mishkin, P.; Clark, J.; Krueger, G.; and Sutskever, I. 2021a. Learning Transferable Visual Models From Natural Language Supervision. In Meila, M.; and Zhang, T., eds., *Proceedings of the 38th International Conference on Machine Learning, ICML 2021, 18-24 July 2021, Virtual Event*, volume 139 of *Proceedings of Machine Learning Research*, 8748–8763. PMLR.

Radford, A.; Kim, J. W.; Hallacy, C.; Ramesh, A.; Goh, G.; Agarwal, S.; Sastry, G.; Askell, A.; Mishkin, P.; Clark, J.; et al. 2021b. Learning transferable visual models from natural language supervision. In *International Conference on Machine Learning*, 8748–8763. PMLR.

Ram, A.; Jalal, S.; Jalal, A. S.; and Kumar, M. 2010. A density based algorithm for discovering density varied clusters in large spatial databases. *International Journal of Computer Applications*, 3(6): 1–4.

Robinson, J.; Chuang, C.-Y.; Sra, S.; and Jegelka, S. 2020. Contrastive learning with hard negative samples. *arXiv preprint arXiv:2010.04592*.

Si, L.; Qiang, W.; Li, J.; Xu, F.; and Sun, F. 2022. Multi-view representation learning from local consistency and global alignment. *Neurocomputing*, 501: 727–740.

Tian, Y.; Krishnan, D.; and Isola, P. 2020a. Contrastive multiview coding. In *European conference on computer vision*, 776–794. Springer.

Tian, Y.; Krishnan, D.; and Isola, P. 2020b. Contrastive Multiview Coding. *arXiv:1906.05849*.

Tomasev, N.; Bica, I.; McWilliams, B.; Buesing, L.; Pascanu, R.; Blundell, C.; and Mitrovic, J. 2022. Pushing the limits of self-supervised ResNets: Can we outperform supervised learning without labels on ImageNet? *arXiv preprint arXiv:2201.05119*.

Van der Maaten, L.; and Hinton, G. 2008. Visualizing data using t-SNE. *Journal of machine learning research*, 9(11).

Wang, J.; Mou, L.; Ma, L.; Huang, T.; and Gao, W. 2023. AMSA: Adaptive multimodal learning for sentiment analysis. *ACM Transactions on Multimedia Computing, Communications and Applications*, 19(3s): 1–21.

Wang, J.; Mou, L.; Zheng, C.; and Gao, W. 2024. Image-based freeform handwriting authentication with energy-oriented self-supervised learning. *IEEE Transactions on Multimedia*.

Wang, T.; and Isola, P. 2020. Understanding contrastive representation learning through alignment and uniformity on the hypersphere. In *International Conference on Machine Learning*, 9929–9939. PMLR.

Zbontar, J.; Jing, L.; Misra, I.; LeCun, Y.; and Deny, S. 2021. Barlow twins: Self-supervised learning via redundancy reduction. *arXiv preprint arXiv:2103.03230*.

Zheng, M.; You, S.; Wang, F.; Qian, C.; Zhang, C.; Wang, X.; and Xu, C. 2021. Rssl: Relational self-supervised learning with weak augmentation. *Advances in Neural Information Processing Systems*, 34: 2543–2555.